Analytica Chimica Acta 1143 (2021) 21–30

Contents lists available at ScienceDirect

Analytica Chimica Acta

journal homepage: www.elsevier.com/locate/aca

Toehold-mediated DNA strand displacement-driven super-fast tripedal DNA walker for ultrasensitive and label-free electrochemical detection of ochratoxin A

Yeru Wang [a], Yu Wang [a], Su Liu [b], Wenyu Sun [a], Manru Zhang [b], Long Jiang [b], Minghan Li [a], Jinghua Yu [c], Jiadong Huang [a, c, *]

[a] School of Biological Sciences and Technology, University of Jinan, Jinan, 250022, PR China
[b] School of Water Conservancy and Environment, University of Jinan, Jinan, 250022, PR China
[c] Key Laboratory of Chemical Sensing & Analysis in Universities of Shandong, School of Chemistry and Chemical Engineering, University of Jinan, Jinan, 250022, PR China

HIGHLIGHTS

- This is the first time that CHA-formed tripedal walker has been introduced into DNA biosensors.
- This flexible tripedal DNA walker is capable of walking freely along the tracks on electrode with unconstrained walking range.
- The design of multiple legs has the capacity to weaken the derailment of leg DNA and shorten the moving time on electrode.
- The ultrahigh sensitivity of this biosensor is attributed to superior walking efficiency of tripedal walker.

GRAPHICAL ABSTRACT

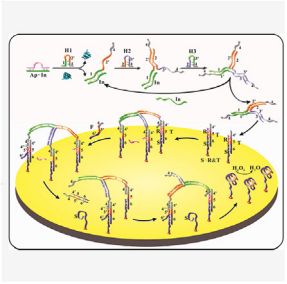

ARTICLE INFO

Article history:
Received 18 September 2020
Received in revised form
28 October 2020
Accepted 13 November 2020
Available online 17 November 2020

Keywords:
DNA walker
Electrochemical biosensor
Toehold-mediated DNA strand displacement
CHA
Ochratoxin A

ABSTRACT

DNA walkers, as intelligent artificial DNA nanomachines, have been widely used as efficient nucleic acid amplification tools that the detection sensitivity can be improved by incorporating DNA walkers into DNA biosensors. Nevertheless, since the premature release or flameout in a region of locally exhausted substrate, the walking efficiency of DNA walkers remains unsatisfactory. In this work, we design a smart tripedal DNA walker that is formed by target-initiated catalyzed hairpin assembly (CHA), which can move along the DNA duplex tracks on electrode driven by toehold-mediated DNA strand displacement (TMSD) for transduction and amplification of electrochemical signals. Emphatically, this flexible tripedal DNA walker is capable of walking freely along the tracks with unconstrained walking range. Moreover, the design of multi-legged walker can weaken the derailment of leg DNA and shorten the moving time on electrode, ensuring the processive walking with high efficiency. Additionally, the persistent walking of tripedal walker is driven by cascading TMSD, which eliminates the defects of high cost and instability of enzyme-assisted amplification technology. Therefore, the tripedal DNA walker-based electrochemical

* Corresponding author. School of Biological Sciences and Technology, University of Jinan, Jinan 250022, PR China.
E-mail address: chm_huangjd@ujn.edu.cn (J. Huang).

https://doi.org/10.1016/j.aca.2020.11.013

biosensor has enormous potential for the applications of OTA detection, and reveals a new avenue for food safety analysis and clinical diagnosis.

1. Introduction

Besides being genetic materials for life, DNA also can be employed as the architectural scaffold for applications in the fields of biomedicine and biosensing [1]. Benefiting from the properties of the DNA materials including of excellent programmability, high stability, and addressability, plenty of artificial DNA nanomachines including DNA tweezers [2], DNA robots [3,4], DNA walkers [5,6], and DNA motors [7] have been fabricated and exploited for biosensing applications. Among these DNA devices, DNA walkers in particular have gained tremendous attention and been recognized as extremely attractive nucleic acid amplification tools that the detection sensitivity can be improved by incorporating DNA walkers into DNA biosensors.

DNA walkers are a group of dynamic DNA machines that can move autonomously along certain oligonucleotide tracks, aiding the transduction and amplification of signals [8]. As the electrode can be used as an ideal interface for DNA walkers owing to its high stability, easy to functionalize, and capable of regeneration, many different DNA walkers-based electrochemical biosensors have been presented for detecting various analytes [9,10]. Generally, DNA walkers running on electrode surfaces can be divided into two types. One utilizes tethered swing arm with one end immobilized on the electrode surface by target-mediated capture or direct chemical interaction, while the other end can walk step by step along the tracks without the dissociation of DNA walkers from the electrode [11,12]. Our prior work also includes the design of an Exonuclease III-powered DNA walker for label-free electrochemical sensing of antibiotics [13]. Nevertheless, the co-assembly of two different DNA strands is required, and the swing arm can only walk along a certain area nearby its foothold that is unfavourable for amplification of electrochemical signal. The other involves a “cleat” inside the walker that allows it to persistently associate with the tracks. For example, Ellington group [14] demonstrates a single-legged walker with a cleat DNA domain, which continuous contacts with the tracks, allowing the catalytic leg to seek out unreacted substrates. Although the simplicity of the walker design, the walking efficiency is not enough because only one leg is running.

According to the existing reports, the walking efficiency can be increased correspondingly as the number of legs increased. For example, Xu and co-authors [15] constructs a Zn (II) ion-driven DNA rolling machine for rapid and ultrasensitive detection of miRNA by using numbers of legs-immobilized AuNPs. Miao and co-authors [16] develop a multipedal AuNPs-DNA walker for highly sensitive detection of circulating tumor cells. Although the walking velocity is enhanced due to the high-speed rolling mode of wheel-like DNA walker, the interlocking force of legs and tracks is unsatisfactory due to the relatively high steric hindrance between nanoparticles and the electrode surfaces, in which the leg DNA is likely to derail the tracks during walking. In addition, the construction of DNA walker involves of the biological labeling and centrifugal separation of nanoparticles, which suffers from the shortcomings of complicated process and hardly-reproducible preparation that may influence the stability and fidelity of results. Therefore, the development of multi-legged DNA walkers with superior walking efficiency, simplified and easily repeated fabrication is still confronting great challenge.

Inspired by the above research results, we intend to design and prepare a smart tripedal DNA walker that is simply formed by taking advantage of catalyzed hairpin assembly (CHA), which can move voluntarily along the DNA duplex tracks on electrode driven by toehold-mediated DNA strand displacement (TMSD). To demonstrate the usability and convenience of the CHA-formed tripedal DNA walker, we select a kind of mycotoxin, ochratoxin A (OTA) as model analyte. Extensive studies have been reported that the excessive usage of OTA causes lethal effects such as teratogenic, nephrotoxic, hepatotoxic, neurotoxic, genotoxic and immunosuppressive effect [17–19]. The conventional OTA assay methods can be generally classified into two categories: instrumental analysis and immunoassay [20]. The instrumental analysis mainly includes high-performance liquid chromatography (HPLC) [21] and HPLC-tandem mass spectrometry (HPLC-MS) [22]. Although the widespread application of these methods, they suffer from the shortcomings of laborious sample pretreatment, sophisticated instrumentation with the need of professional technicians. The immunoassay methods such as enzyme-linked immunosorbent assay (ELISA) [23], and chemiluminescent immunoassay (CLIA) [24] rely on the specific antigen-antibody reaction, which involves of incubation and washing steps that are usually time-consuming and cumbersome. Therefore, it is urgent to develop simple, rapid, and convenient, and highly sensitive strategies for determining trace amounts of OTA in foodstuffs.

In this regard, we report here a smart TMSD-driven tripedal DNA walker which is integrated with electrochemical biosensor for ultrasensitive detection of OTA. To the best of our knowledge, this is the first time that CHA is directly utilized to create tripedal walker that is driven by TMSD for transduction and amplification of electrochemical signals. This smart tripedal DNA walker features with several aspects. Above all, our designed DNA walker is capable of walking freely along the tracks that the walking range is unconstrained. Secondly, the leg DNA is able to walk allodially along the tracks without the dissociation of it from the tracks due to the large interlocking force of legs and tracks of tripedal walker, thus the processive walking with high efficiency can be ensured. Thirdly, the construction of tripedal walker is simple and easy repeated, which do not require the immobilization of leg DNA on the tracks or biological labeling of nanoparticles. On the basis of the above points, this constructed tripedal walker is expected to enable to solve the problems of the existing DNA walker including premature release or flameout in a region of locally exhausted substrate. Besides, benefiting from the superior walking efficiency of this tripedal walker, ultrahigh sensitivity is achieved for electrochemical assay of OTA due to the property of signal amplification of DNA walker. In addition, the persistent walking of tripedal walker is driven by cascading TMSD, which eliminates the defects of high cost and instability of enzyme-assisted amplification technology. Furthermore, G-quadruplex/hemin complex is used as biocatalyst for achieving label-free electrochemical detection, which offers the advantages of low reagent cost and amplified detection of OTA at low levels. Hence, the proposed super-fast tripedal DNA walker-based electrochemical biosensor indeed provides a powerful tool for detecting trace amounts of OTA and related food safety analysis.

2. Experimental section

2.1. Materials and chemical

The DNA oligonucleotides sequences included in Table 1 were purified and synthesized by HPLC by Shanghai Shenggong Biotechnology Co. Ltd (Shanghai, China). Ochratoxin A (OTA) and Zearalenone (ZEN) were obtained from Aladdin Biochemical Technology Co. Ltd (Shanghai, China). Aflatoxin B1 (AFB1) and Ochratoxin B (OTB) were obtained from Sigma-Aldrich (Shanghai, China). 6-mercapto-L-hexanol (MCH); EDTA and tris (2-carboxyethyl) phosphine hydrochloride (TCEP) were purchased from Aladdin Chemistry Co. Ltd (Shanghai, China). The rest are analytical grade, purchased from Sinopharm Chemical Reagent Co. Ltd (Beijing, China). Hemin (1 mM) was prepared by dimethyl sulfoxide (DMSO) and stored at −20 °C in dark.

The underlined part of H1, H2, H3 is the toehold sequence of tripedal DNA walker. The 3' terminus of the S was decorated with the sulfhydryl group (−$(CH_2)_6$−SH). The intermediate italic sequence of T combines with the R, and the underlined part hybridizes with the underlined part of H1, H2 and H3, and the bold part hybridizes with the bold part of S.

2.2. Apparatus

Cyclic voltammetry (CV), Electrochemical impedance spectroscopy (EIS) and differential pulse voltammetry (DPV) experiments were conducted on CHI 660D Electrochemical workstation (Shanghai Chenhua Instrument Co., LTD., China). DPV, CV and EIS were measured using a three-electrode system consisting of a saturated Ag/AgCl reference electrode with platinum wire as the auxiliary electrode and modified or bare gold electrode (2 mm in diameter) as the working electrode. Absorption spectra were conducted on a UV2600 UV−vis spectrophotometer (Shimadzu international trading Co. Ltd., Japan).

2.3. Fabrication of the sensing interface of electrode

Firstly, the gold electrodes were carefully polished to a mirror surface with 0.5 and 0.05 μm alumina slurries, and cleansed immersed in the freshly prepared piranha solution (H_2O_2/H_2SO_4, 1:3) for 2 h with three times. The gold electrodes were then washed with ultra-pure water and ultrasonic with anhydrous ethanol for 5 min respectively, and it was dried in air.

In the process of modifying the electrode, the S-R&T should have been prepared primarily. R (10 μL, 100 μM), T (10 μL, 100 μM), S (10 μL, 100 μM) with 10 mM Tris-HCl buffer solution (containing 1 M of NaCl, 1 mM of EDTA, 1 mM of TCEP, pH 7.4) were blended, and which had been reaction for 2 h at 37 °C in thermostatic waterbath. This mixture was dropped onto the surface of the electrodes and self-assembled overnight in an incubator at 37 °C. The incubated electrodes were then washed with phosphate buffered saline containing 0.14 M of NaCl (PBS, 10 mM, pH 7.4) to remove excess S-R&T. To conquer nonspecific adsorption effect, 1 mM MCH solution was used to block the unoccupied sites of the electrodes. Finally, the modificatory electrodes were washed with PBS for three times and stored in a refrigerator at 4 °C for later use.

2.4. Preparation of tripedal DNA walker

Aptamer-initiator (Ap-In) duplex were prepared by annealing firstly, aptamer (5 μL, 25 μM), initiator (5 μL, 25 μM) and reaction buffer (50 mM of Tris-HCl, 50 mM of KCl, 5 mM of $MgCl_2$, pH 7.4) were added in 30 μL ultrapure water. The mixture was heated to 95 °C and kept this temperature for 5 min, then gradually cooling to room temperature to obtain the Ap-In. The H1, H2, H3 were quenched in reaction buffer before catalytic hairpin assembly, and then the tripedal DNA walkers were prepared. Mixing 6 μL 2.5 μM Ap-In, 6 μL 12.5 μM H1, H2, H3, 15 μL 100 μM F, 6 μL 100 ng/mL OTA, with 12 μL 5 × reaction buffer and 3 μL H_2O, incubated at 37 °C for 2 h to obtained mixture 1.

2.5. Electrochemical measurements

The mixture 1 was dropped onto the modified electrodes surface and incubated in incubator for 50 min to obtain exposed G-quadruplets by TMSD reaction on the electrode surface. Then, the electrodes were immersed in 1 mM hemin for 30 min to from the hemin/G-quadruplets which as a DNAzyme similar to horseradish peroxidase. Finally, the electrodes were washed with PBS for three times. All DPV data were recorded at room temperature of 10 mM PBS (containing 140 mM of NaCl, 5 mM of KCl, 1 mM of $MgCl_2$, 1 mM of $CaCl_2$, and pH 7.4). DPV was recorded within the potential range of modulation amplitude of 50 mV, scanning rate of 50 mV s^{-1}, step potential of 0.83 mV, and potential range of 0 to −0.5 V. CV scanning rate was 50 mV s^{-1} in 10 mM PBS (pH 7.4), containing 0.25 of mM KCl and 5 mM of $[Fe(CN)_6]^{3-/4-}$. EIS was conducted in an aqueous solution of 0.25 mM of KCl containing 5 mM of $[Fe(CN)_6]^{3-/4-}$, with frequency range of 0.1 Hz−100 kHz and amplitude of 5 mV [25].

2.6. Polyacrylamide-gel electrophoresis (PAGE) characterization

After mixing the DNA samples with the DNA loading buffer (volume ratio: 5:1), polyacrylamide gel electrophoresis (PAGE) was carried out with 1 × TBE buffer (pH 8.0). The electrophoresis time was 100 V and the electrophoresis time was 60 min. The dynamic DNA assembly products of the newly prepared 8% polyacrylamide gel were analyzed.

Table 1
DNA oligonucleotides sequences used in this work.

Oligonucleotide name	Sequence (5′ to 3′) description
Aptamer	GATCGGGTGTGGGTGGCGTAAAGGGAGCATCGGACA
Initiator	GTGCCCTGTCCGATGCAATGACACCCGATC
H1	GATCGGGTGTCGTTGCATCGGACAGGGCACCCGATCCGACCCGTGCCCTGACCGCTGTAGCGACGCGTTCAT
H2	CTACAGCGGTCGGGGTACGGGTCGGATCGGATGCAACGATACCCGATCCGACCCCTAGTCCGACGCGTTCAT
H3	AACTAGGGGTCGGATCGGGTGTCGTTGCATGTGCCCTGTCCGATGCAACGACACCCGATCCGACGCGTTCAT
S	**GAGGGTGGGGAGGGT**GGGGCCAA−$(CH_2)_6$−SH
R	*TCATGACTCT*
T	**ACCCTCCCCACCCTC***AGAGTCATGA*ACGCGTCG
F	GTTCATGACTCTGAGGGTGGGGAGGGT

2.7. Analysis of OTA in actual samples

Red wine was taken as the actual sample for OTA determination at different concentrations. A filtration process was used to remove the sediment from the wine sample. The actual red wine sample to be tested was adjusted to pH 7.4 and diluted 20 times, and then further study was conducted. OTA of different concentrations (0.10, 0.50, 1.0, 5.0, and 10 ng/mL) were added to the sample to make a standard sample. The following operation is the same as above.

3. Results and discussion

3.1. Principle of the tripedal DNA walker-based electrochemical biosensor

The working principle of the proposed super-fast tripedal DNA walker-based electrochemical biosensor for OTA quantification is illustrated in Scheme 1. The double-stranded DNA complexes (S-R&T) are immobilized on gold electrode surface via Au-sulfur self-assembly to constitute the sensing interface, which are used as the tracks supplying the running of tripedal walkers. S decorated with sulfhydryl group at the 3′-ternimus contains hemin aptamer sequence that can form G-quadruplex DNAzyme in the presence of K^+ and hemin. T is comprised of the annealing sequence with S and R, in which a toehold domain with 8 nt (the gray region in Scheme 1) at the 3′-end is designed to ensure the smooth running of strand displacement amplification (SDA) reaction. F as the fuelled DNA can hybridize with the toehold domain (6 nt, the red region in Scheme 1) in the middle of T that is blocked by S and R beforehand, which results in the release of one “leg” of tripedal walkers that can sequentially seek out other unreacted substrates through toehold-mediated DNA strand displacement (TMSD) reaction. Our sensing system consists of target-induced formation of tripedal walker via CHA in the homogeneous solution and the following running autonomously along the tracks driven by TMSD on electrode to release the electrochemical signal. When target OTA is added into the reaction solution including aptamer-initiator (Ap-In) duplex, H1, H2, and H3, the specific recognition of OTA and its aptamer induces the release of initiator, which as a single-stranded catalyst initiates the cyclic CHA reaction. As a result, the continuous assembly between three hairpins (H1, H2, and H3) conducts to form stable tripedal DNA walker. Subsequently, the formed tripedal walker is tethered along the tracks on electrode surface through the hybridization of three legs of walker with short extended single-strand domain (8 nt, the gray region in Scheme 1) at the 3′ terminus of T, thus TMSD reaction is activated that supplies the steady walking of tripedal walker on the tracks. After the association of one leg of walker with the tracks, R in the double-stranded complex (S-R&T) is displaced, exposing the toehold domain (the red region in Scheme 1) in the middle of T, thus F attaches to the exposed domain and completely hybridizes with T through a branch migration process accompanied with the displacement of S and the leg of walker, remaining the single-stranded S on electrode surface. Immediately, the unchained leg searches for another new track, allowing to processive walking along the tracks driven by cascading TMSDs. Particularly, the tripedal walker can move autonomously on the tracks at high speed without the dissociation of the walker from the tracks, which is attributed to the persistent contact of at least one leg with tracks that allows the catalytic leg to more readily seek out unreacted substrates. After the continuous consumption of the tracks by highly efficient tripedal walker, numerous of single chain S is liberated, in the presence of K^+, the G-quadruplex/hemin complex that can act as DNAzyme mimicking peroxidase. Consequently, the reduction of H_2O_2 catalyzed by G-quadruplex DNAzyme can obtain an obvious strong current signal. On the contrary, when OTA is absent in the reaction system, S is blocked by T and unavailable for binding with hemin, thus the background signal is suppressed as expected. In contrast, when the target OTA is not present, initiator was blocked and the DNA walker machine did not work as expected, thus a negligible current signal could be

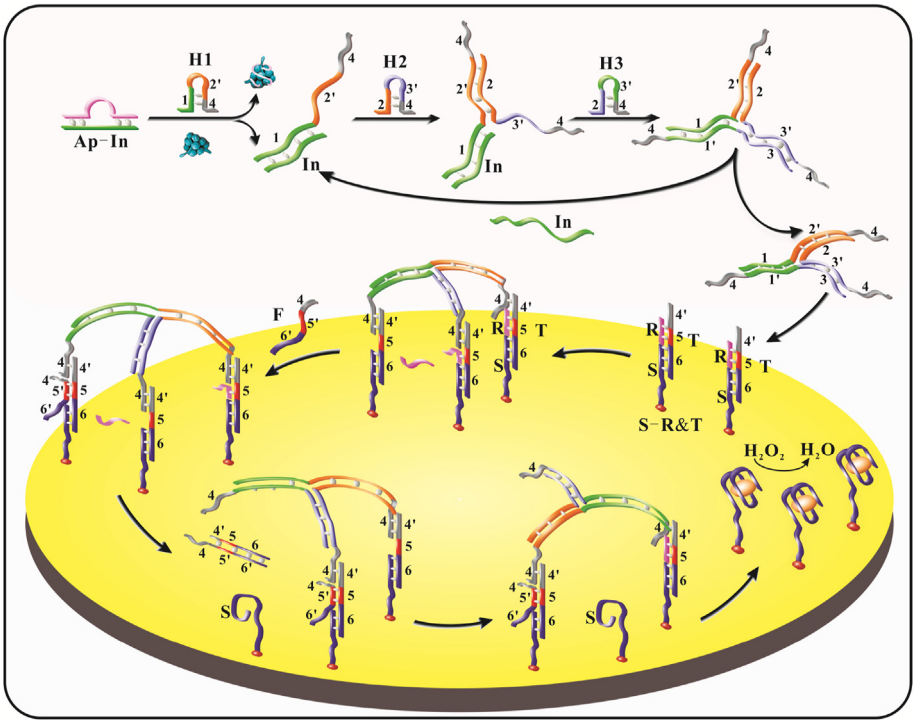

Scheme 1. Schematic illustration of the label-free electrochemical biosensor for detecting OTA based on super-fast tripedal DNA walker.

obtained. Therefore, the constructed tripedal DNA walker-based electrochemical biosensor holds the potential to be applied for detecting OTA at low levels.

3.2. Feasibility study of the proposed biosensor

In order to demonstrate the feasibility of TMSD-driven electrochemical sensing strategy based on tripedal DNA walk for OTA detection, DPV was first used for electrochemical characterization, and the results obtained in a series of control experiments were shown in Fig. 1A. To proof the feasibility of the TMSD-driven tripedal DNA walker-based electrochemical sensing strategy for OTA detection, DPV was used for electrochemical characterization, and the results obtained in a series of control experiments were shown in Fig. 1A. For the positive sample (10 ng/mL OTA), an obvious strong current signal with a DPV peak at around −0.35 V was observed, indicating tripedal DNA walkers were formed via OTA-mediated CHA that initiated cascading TMSD, thus numerous of G-quadruplex/hemin complex generated and catalyzed the reduction of H_2O_2 that released a remarkably obvious current signal (curve a). In contrast, a negligible DPV peak was observed for the blank sample, which signifying the formation of tripedal DNA walker and the following TMSD reaction and resulting generation of G-quadruplex/hemin complex was specifically induced by the binding of OTA and its aptamer (curve b). Moreover, we also verified other control experiments in the proof-of-concept experiments, including Ap-In duplex, H1, F, or non-target AFB1. When 10 ng/mL OTA was incubated with the reaction system in the absence of Ap-In duplex, there was a very weak current signal similar to that of the blank sample (curve c). This implying H1, H2, and H3 were stable in reaction solution that CHA reaction couldn't conduct in the absence of the initiator functioned as a single-stranded catalyst. When incubated 10 ng/mL OTA with the reaction system in the absence of H2, a slightly stronger current peak was observed compared with that of the blank sample, which suggesting the walking velocity of only single-legged DNA walker was not as fast as the present tripedal walker that was closely related to the signal amplification (curve d). Additionally, after the incubation of 10 ng/mL OTA with the reaction system in the absence of H3, it was observed that a moderate current peak appeared in the DPV curve, manifesting the walking efficiency of two-legged DNA walker was higher than that of single-legged DNA walker, while lower than tripedal walker, this is, the walking efficiency increased correspondingly as the number of legs increased (curve e). This might be attributed that multi-legged DNA walker weakened the detailing of leg DNA and shortened the running time that leads to significant amplification of the signal outputs. In addition, when non-target AFB1 replaced OTA, an undetectable DPV peak occurs, indicating that the constructed biosensor has high specificity (curve f). On the basis of these above results, the proposed tripedal DNA walker-based electrochemical strategy was expected to detect OTA with high sensitivity and specificity.

We also performed the absorption analysis to further verify the feasibility of TMSD-driven tripedal DNA walker for OTA assay. As shown in Fig. 1B, for the positive sample, there was an intense characteristic absorption peak at ~425 nm, manifesting OTA-activated tripedal walker driven by TMSD induced the formation of abundant of G-quadruplex DNAzyme that displayed excellent catalytic activity toward the H_2O_2-aided oxidation of TMB (curve a). In stark contrast, for the blank sample, it was observed that an extremely weak absorption peak was obtained (curve b), which implying the hemin aptamer was totally blocked in double-stranded complexes of S-R&T that couldn't assemble into G-quadruplex structure in the presence of K^+ and hemin. This implying the formation of G-quadruplex DNAzyme was caused by the specific recognition of OTA and its aptamer rather than other uncontrolled factors. Besides, G-quadruplex DNAzyme-catalyzed oxidation of TMB via H_2O_2 enables to generate a colored signal readout that can be easily discerned by the naked eye. The inset displaying a corresponding color changes for the positive sample and the blank sample, which was consistent with the absorption spectral measurements. In brief, these data further confirmed the feasibility of tripedal DNA walker-based sensing strategy for OTA detection.

3.3. PAGE validation

As a proof-of-concept experiment, the mechanism of TMSD-driven tripedal DNA walker for OTA detection was investigated by PAGE analysis, and the results were depicted in Fig. 2. Lane M was the DNA marker with different molecular weights. The band at Lane 1 represented Ap-In duplex prepared by annealing aptamer with initiator. After the incubation of OTA with Ap-In duplex, the brightness of the band at the position of Ap-In obviously decreased, indicating the specific binding of OTA and its aptamer as expected. Lands 3, 4, 5 displayed corresponding bands of H1, H2, and H3, respectively. As seen from Lanes 6–8, the assembly process of tripedal DNA walker could be clearly observed. After incubation of OTA with Ap-In duplex and H1, we observed from Lane 6 that a new band with high molecular weight appeared on the image,

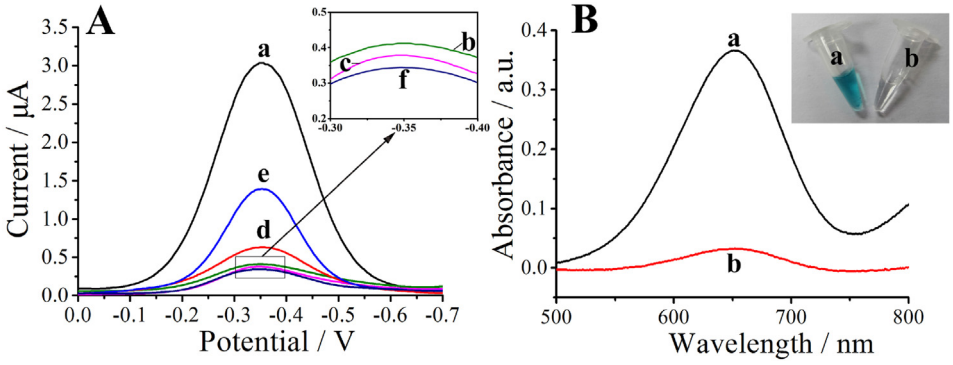

Fig. 1. (A) The DPV responses of the biosensor obtained upon analyzing 10 ng/mL OTA (curve a). Curves b-g were for the control experiments which were performed with no OTA (b), 10 ng/mL OTA without Ap-In duplex (c), 10 ng/mL OTA without H2 (d), 10 ng/mL OTA without H3 (e), and non-target AFB1 in place of OTA (f). DPV measurements were performed in 10 mM PBS (pH 7.4) containing 2 mM H_2O_2 and 5 mM K^+. (B) The absorption spectral responses of tripedal DNA walker-based biosensor obtained upon analyzing the positive sample (10 ng/mL OTA, curve a) and the blank sample (curve b). Experiments were performed in TMB-H_2O_2 reaction system. The inset shows a naked-eye color difference and the corresponding products. (For interpretation of the references to color in this figure legend, the reader is referred to the Web version of this article.)

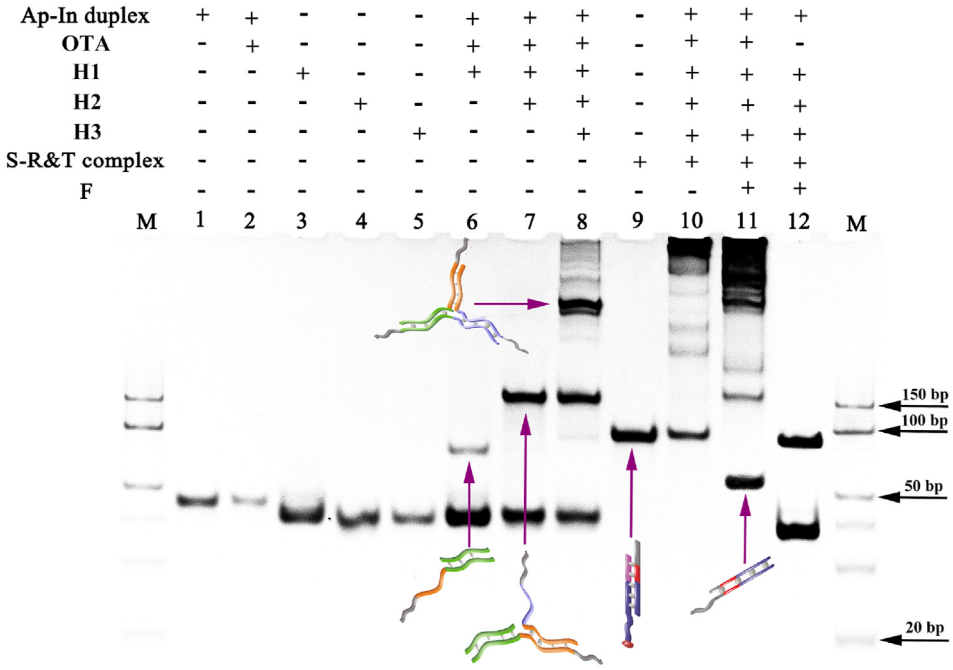

Fig. 2. Gel electrophoresis image of TMSD-driven tripedal walker for OTA assay.

suggesting the binding of OTA and its aptamer resulted in the release of initiator followed by the hybridization with H1 and the formation of In–H1 duplex. After incubation of OTA with Ap-In duplex, H1, and H2, a fresh band with higher molecular weight than that of Lane 6 was observed, which indicating the opened H1 combined with H2 and formed In–H1–H2 assemblies. After incubation of OTA with Ap-In duplex, H1, H2, and H3, there was another new band with relatively slower migration rate (Lane 8). This demonstrated a continuous assembly step between H1, H2, and H3 smoothly conducted and formed stable duplex DNA assemblies with branching connections, which could be supported by the previous report about CHA-induced "Y" shape DNA nanostructure [26–28]. Land 9 represented a double-stranded DNA complex formed by annealing R, T with S. After incubation of OTA with Ap-In duplex, H1, H2, H3, and S-R&T, the brightness of the band characteristic for S-R&T became weaker, and certain new bands with extremely slow migration rate appeared on the image (Lane 10). This implying the generated tripedal walker was tethered on S-R&T through the hybridization of three legs of walker with short extended single-strand domain at the 3' terminus of T, forming bulky DNA assemblies with large molecular weight. After incubation of OTA with Ap-In duplex, H1, H2, H3, S-R&T, and F (the positive sample), the top bands showed a downward trend, and the band at the position of S-R&T disappeared accompanied with the appearance of a new band with low molecular weight (Lane 11). This was attributed that the tripedal DNA walker initiated cascading TMSD with the aid of F, which resulted in the partially unwinding of the bulky DNA assemblies and the formation of F-T duplex. In contrast, for the blank sample, it was found that Lane 12 displayed two bright bands characteristic for S-R&T and three hairpins. These data gave the immediate evidence only the addition of target OTA can induce the formation of tripedal DNA walker that ignites cascading TMSD reaction for signal output.

3.4. Characterization of the modified electrodes

CV measurements were constructed in 5.0 mM $[Fe(CN)_6]^{3-/4-}$ to monitor the modification of the electrochemical sensing interface. As shown in Fig. 3A, a distinctly declined current signal (curve b) for the electrode modified with S-R&T duplex was observed compared with that of the bare Au electrode (curve a). Seen from curve c, for the MCH/S-R&T complex/Au electrode, the current signal was further decreased, which was attributed that the electron transport between the electrode and solution was mostly hindered by nucleic acids and MCH molecules with poor conductivity. Nevertheless, when incubated MCH/S-R&T complex/Au electrode with the reaction system in the presence of 10 ng/mL OTA, the peak current was dramatically increased and the peak-to-peak separation declined in the CV curve (curve d). This signifying target-initiated tripedal DNA walker consumed large amounts of S-R&T complex powered by TMSD that leaded to the enhanced electron transfer efficiency. Furthermore, EIS measurements were also implemented to further supervise the fabrication process of the modified electrode. As depicted in Fig. 3B, it was observed that the impedance curve of the bare Au electrode had almost no semi-circle (curve a). With the stepwise modification of S-R&T complex (curve b) and MCH (curve c), the diameter of the semi-circle (Ret) correspondently increased. However, when treated the modified electrode with the reaction system in the presence of target OTA, the Ret showed an obvious decrease owing to the consumption of S-R&T complex induced by tripedal walker-activated cascading TMSD (curve d). All above data verified the successful construction of OTA electrochemical sensing interface.

3.5. Optimization of the experimental conditions

In order to make the electrochemical biosensor have the best analytical performance, a series of experimental conditions, such as the concentrations of Ap-In duplex, H1/H2/H3, H_2O_2, and S-R&T complex and walking times of tripedal DNA walker were optimized, and the results were shown in Fig. 4. Fig. 4A depicted the effect of Ap-In duplex concentration on the current signal of the biosensor. We observed the current intensity of positive sample increased gradually with the increase concentration of Ap-In duplex and then

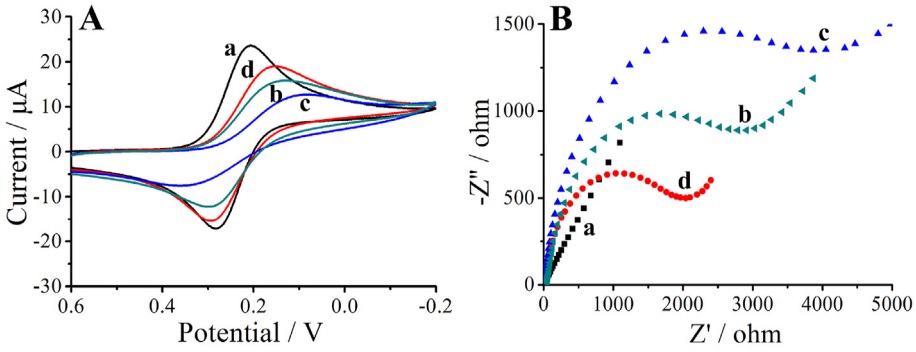

Fig. 3. CVs (A) and EISs (B) obtained for the bare Au electrode (a), S-R&T complex/Au (b), MCH/S-R&T complex/Au (c), and the modified electrode upon analyzing 10 ng/mL OTA (d). CV and EIS measurements were performed in 10 mM PBS (pH 7.4) containing 0.25 mM KCl and 5.0 mM $[Fe(CN)_6]^{3-/4-}$.

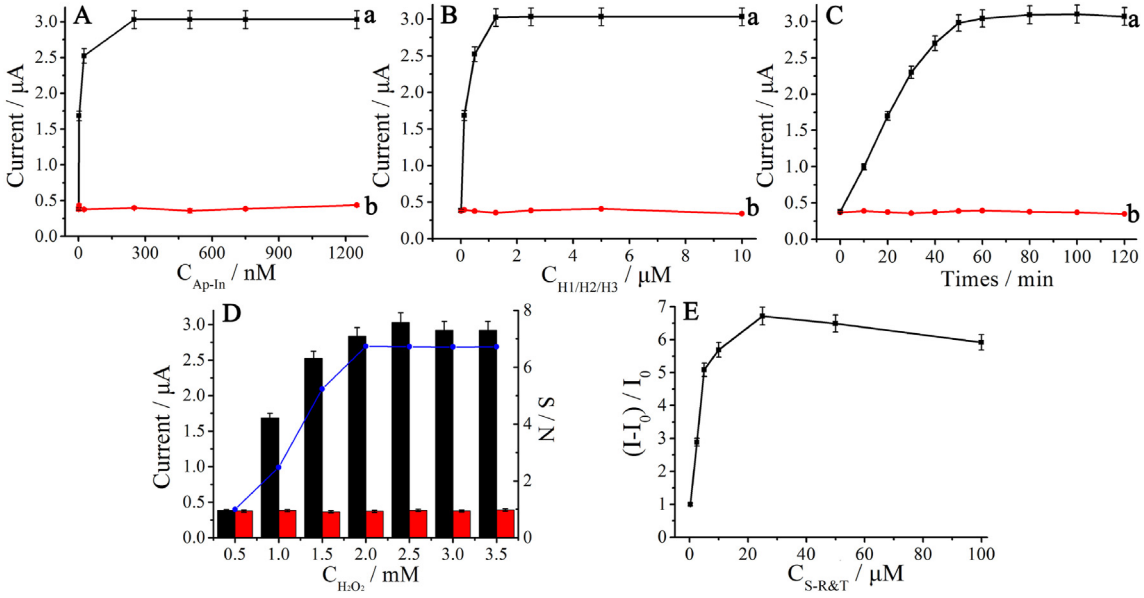

Fig. 4. (A) Effect of the concentration of Ap-In duplex on the current signal of the biosensor in the presence (curve a) and absence (curve b) of 10 ng/mL OTA; (B) Effect of the concentration of H1/H2/H3 on the current signal of the biosensor in the presence (curve a) and absence (curve b) of 10 ng/mL OTA; (C) Effect of the walking time of tripedal DNA walker on the current signal of the biosensor in the presence (curve a) and absence (curve b) of 10 ng/mL OTA; (D) Effect of the concentration of H_2O_2 on the current signal of the biosensor in the presence (the black bar) and absence (the red bar) of 10 ng/mL OTA. Error bars are standard deviations across three repetitive experiments; (E) Effect of the concentration of S-R&T complex on the current signal of the biosensor. (For interpretation of the references to color in this figure legend, the reader is referred to the Web version of this article.)

tended to be constant when the concentration reached to 250 nM (curve a), while the blank sample showed little change (curve b). So, the concentration of 250 nM was selected as the optimal Ap-In duplex concentration. As shown in Fig. 4B, the current signal was intensified with increasing of H1 concentration and experienced almost no change when H1/H2/H3 concentration reached to 1.25 μM (curve a). Nevertheless, the current intensity of the blank sample changed little (curve b). Therefore, 1.25 μM was selected as the optimal concentration for H1/H2/H3. It was of great importance for the running time of tripedal DNA walker to speedy detection. As seen in Fig. 4C, the electrodes incubated with the positive samples showed intensified current signals with increasing of walking time and little changed when the time reached 50 min (curve a). There were no obvious changes for the current signals of the blank samples (curve b). Hence, the walking time of the tripedal DNA walker was chosen as 50 min, which was superior to single or bipedal DNA walker [29–31]. Additionally, it was of great importance for the concentration of H_2O_2 to the signal-to-noise (S/N) of the proposed strategy. The concentration of H_2O_2 was studied and the current signals of positive samples and blank samples were detected. It was found from Fig. 4D that the concentration of 2 mM gave the highest S/N (6.737). Thus, 2 mM were chosen as the optimal concentration for H_2O_2 in the following experiments. Furthermore, the amount of S-R&T complex immobilized on electrode surface had an effect on the walking efficiency of tripedal DNA walker. The concentration of S-R&T complex also was optimized on the basis of the current signal upon analyzing the positive sample and the blank sample (Fig. 4E). We investigated the variances of the $(I-I_0)/I_0$ value with different concentrations of S-R&T, where I and I_0 were the current intensity at −0.35 V in the presence and absence of OTA, respectively. The value of $(I-I_0)/I_0$ increased continuously with increasing of S-R&T concentration, and then leveled off when the concentration of S-R&T was reached to 25 μM. As the concentrations of S-R&T continuously increased, the current signal declined, which was attributed that the immobilized DNA on electrode surfaces was too crowded that influenced the hybridization efficiency between the tripedal walker and S-R&T. Hence, 25 μM was selected as the optimal S-R&T concentrations for the

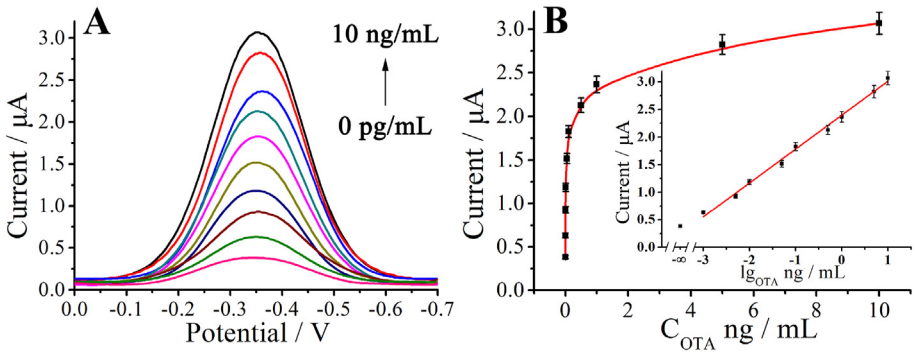

Fig. 5. (A) DPV responses of the biosensor to different concentrations of OTA (from 0 pg/mL to 10 ng/mL: 0, 1.0×10^{-3}, 5.0×10^{-3}, 1.0×10^{-2}, 5.0×10^{-2}, 1.0×10^{-1}, 5.0×10^{-1}, 1.0, 5.0, 10 ng/mL). (B) The calibration curve of DPV peak intensity at around −0.35 V for different concentrations of OTA. Inset is the plot of the DPV peak intensity at around −0.35 V versus the logarithm of OTA concentrations. Error bars are standard deviations across three repetitive experiments.

Table 2
Comparison of different methods for OTA determination.

Method	Detection range (ng/mL)	Detection limit (ng/mL)	Reference
ELISA	5.00×10^{-3} - 6.40×10^{-1}	4.00×10^{-2}	[33]
ELISA	1.25×10^{-2} - 1.50×10^{-1}	1.78×10^{-2}	[34]
Fluorescent assay	5.00×10^{-2} - 2.00×10^{1}	1.30×10^{-2}	[35]
Fluorescent assay	5.00×10^{-2} - 1.00×10^{2}	2.00×10^{-2}	[36]
Electrochemiluminescence assay	1.00×10^{-2} - 1.00×10^{2}	4.28×10^{-3}	[37]
Electrochemiluminescence assay	1.00×10^{-2} - $1.00 \times 10^{\circ}0$	2.00×10^{-3}	[38]
Electrochemical assay	1.00×10^{-2} - 1.00×10^{1}	3.00×10^{-3}	[39]
Electrochemical assay	1.00×10^{-1} - 1.00×10^{1}	3.00×10^{-2}	[40]
Electrochemical assay	1.00×10^{-3} - 1.00×10^{1}	9.50×10^{-4}	This work

subsequent experiments. We also studied the effect of pH on the catalytic activity of G-quadruplet/hemin DNAzyme by TMB colorimetry and the results were shown in Fig. S1. It was observed that the highest catalytic activity was achieved when the pH was 7.4, and the catalytic activity was rather lower when the buffer was acidic (pH < 6) or alkaline (pH > 8.5). This result was consistent with the conclusion reported in previous work [32].

3.6. Analytical performances of the biosensor for OTA assay

Under the optimal experiments, the ability of the proposed electrochemical biosensor for quantitative assay of OTA was studied. Fig. 5A depicted typical DPV responses of the biosensor upon analyzing OTA of varying concentrations. We observed the current signal increased accordingly with the increase of OTA concentration from 0 pg/mL to 10 ng/mL. In addition, the plot of the peak current intensities versus the logarithm of OTA concentrations had a good linear relationship in the concentration range 1 pg/mL - 10 ng/mL, that was, over 4 orders of magnitude (Fig. 5B). The regression equation was $I = 2.4 + 0.61 \times \lg C_{OTA}$, the correlation coefficient was 0.997, where I and C represented the peak current intensity and OTA concentration (ng/mL), respectively. The detection limit (LOD) was calculated to be 0.95 pg/mL according to the 3σ rules. Additionally, the relative standard deviations (RSDs) of current signal at −0.35 V were 2%, 1%, 1%, 1%, in four repetitive assays of 5.0×10^{-3}, 5.0×10^{-2}, 5.0×10^{-1}, and 5.0 ng/mL of OTA, which manifested the excellent reproducibility of this biosensor. In addition, the performance of OTA quantitative analysis of existing electrochemical biosensors was compared with some previously reported methods. As shown in Table 2, our biosensor showed improved detection limit and expanded detection range in comparison with these methods. The ultrahigh sensitivity could be ascribed to superior walking efficiency of the constructed tripedal DNA walker. As a result, our electrochemical biosensor is capable for profiling OTA with low abundance in foodstuffs.

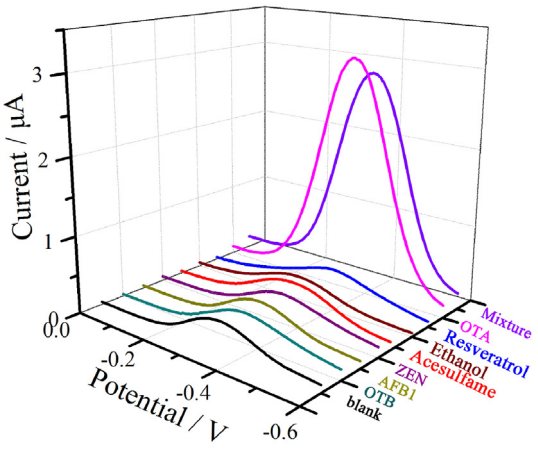

Fig. 6. DPV responses of the biosensor obtained towards the detection of different substances. The concentration of OTA is 10 ng/mL. The concentrations of non-target substances are 100 ng/mL. Error bars are the standard deviations across three repetitive experiments.

The selectivity of sensing strategy is an essential parameter during practical applications in complicated samples. We examined the specificity of this biosensor upon analyzing target OTA and several kinds of non-target substances including Ochratoxin B (OTB), Aflatoxin B1 (AFB1), Zearalenone (ZEN), Acesulfame, Ethanol and Resveratrol, respectively under the same experimental conditions. As shown in Fig. 6, a remarkably strong current signal was observed only when OTA exists in the reaction system, while the current signals were negligible in the presence of even 10-fold excess of other substances. These observations confirmed the

Table 3
Application of the electrochemical biosensor to detect OTA in wine and comparison with HPLC detection.

Spiked amount (ng/mL)	Found amount (ng/mL) (±SD, n = 5)		Recovery (%)	
	Our biosensor	HPLC	Our biosensor	HPLC
10	9.850 ± 0.069	9.870 ± 0.084	98.45	98.27
5.0	4.980 ± 0.007	4.960 ± 0.008	99.58	99.26
1.0	0.9760 ± 0.009	0.9830 ± 0.005	97.30	98.40
0.50	0.5100 ± 0.011	0.5150 ± 0.009	103.2	102.7
0.10	0.09590 ± 0.002	0.09660 ± 0.002	96.40	96.90

ultrahigh specificity of the proposed biosensor for OTA detection. Further studies were conducted to investigate the stability of the biosensor, and the results were shown in Fig. S2 in the supporting information. We stored the working electrode at 4 °C for 0, 5, 10, and 15 days, and then detected 10 ng/mL OTA under the same experimental conditions. The results showed that the current response was similar and the original DPV response to OTA was preserved at least 97%, suggesting the constructed biosensor had very good stability.

3.7. Application of the biosensor in actual samples

In order to further demonstrate the practicability of the constructed biosensor, the quantitative assay of OTA in actual red wine samples was examined using this biosensor. The red wine samples were spiked with 5 different concentrations of OTA (0.10, 0.50, 1.0, 5.0, and 10 ng/mL) and detected without any pretreatment except dilution with buffer. These spiked samples were also measured by classical HPLC. The results were shown in Table 3. We observed that the data obtained using our biosensor was consistent with that obtained by HPLC. Besides, the recoveries of our strategy were in the range of 96.40–103.2% with relative standard deviations (RSDs) in the range of 0.140–1.18%. The results show that the biosensor can be used in complex sample analysis with high reliability and accuracy.

4. Conclusions

The current study describes a super-fast CHA-formed tripedal DNA walker driven by TMSD for amplified electrochemical detection of OTA. Our smart tripedal DNA walker has several highlights. First, the design of multiple legs has the capacity to weaken the derailment of leg DNA and shorten the moving time on electrode, ensuring the processive walking of DNA walker with high efficiency. Second, this tripedal walker is capable of walking freely along the tracks on electrode that the walking range is unconstrained. Third, unlike previously reported DNA walkers, the preparation of tripedal walker is simple and easy repeated, which do not require the immobilization of leg DNA on the tracks or biological labeling of nanoparticals. Lastly, the persistent walking of tripedal walker is driven by cascading TMSD, which eliminates the defects of high cost and instability of enzyme-assisted amplification technology. Owing to the above highlights of this tripedal walker, this efficient tripedal walker is expected to be capable of solving the problems of the previous DNA walker including being prone to release prematurely or flameout in a region of locally exhausted substrate. To the best of our knowledge, this is the first time that CHA-formed tripedal walker is introduced into DNA biosensors. Using OTA as a model analyte, the proposed electrochemical biosensor demonstrates excellent sensitivity and specificity toward OTA with detection limit as low as 0.95 pg/mL. In addition, this biosensor has been successfully applied for practical samples analysis. Furthermore, the tripedal DNA walker-based sensing strategy can be readily expanded as a universal platform for the detection of a variety of analytes by changing the affinity probe pairs. Overall, the developed biosensor could pave a prospective way for application in bioanalysis.

CRediT authorship contribution statement

Yeru Wang: Data curation, Writing - original draft, Writing - review & editing. **Yu Wang:** Methodology, Writing - review & editing. **Su Liu:** Methodology, Validation. **Wenyu Sun:** Methodology, Validation. **Manru Zhang:** Methodology, Validation. **Long Jiang:** Methodology, Validation. **Minghan Li:** Methodology, Validation. **Jinghua Yu:** Methodology, Visualization. **Jiadong Huang:** Conceptualization, Validation, Supervision, Writing - review & editing.

Declaration of competing interest

The authors declare that they have no known competing financial interests or personal relationships that could have appeared to influence the work reported in this paper.

Acknowledgements

This work was supported by Jinan City “20 Items in Colleges” Funds (2019GXRC056), the Primary Research & Development Plan of Shandong Province (2017GSF220009), the Program for Taishan Scholar of Shandong Province (ts201712048), and the Project of Shandong Province Higher Educational Science and Technology Program (J18KA109).

Appendix A. Supplementary data

Supplementary data to this article can be found online at https://doi.org/10.1016/j.aca.2020.11.013.

References

[1] N.C. Seeman, H.F. Sleiman, DNA nanotechnology, Nat. Rev. Mater. 3 (2017) 17068.
[2] L. Zhou, M. Gao, W. Fu, Y. Wang, M. Chen, Three-dimensional DNA tweezers serve as modular DNA intelligent machines for detection and regulation of intracellular microRNA, Sci. Adv. 6 (2020), eabb0695.
[3] A. Halder, Y. Sun, Biocompatible propulsion for biomedical micro/nano robotics, Biosens. Bioelectron. 139 (2019) 111334.
[4] Y. Chang, Z. Wu, Q. Sun, Y. Zhuo, Y. Chai, R. Yuan, Simply constructed and highly efficient classified cargo-discharge DNA robot: a DNA walking nanomachine platform for ultrasensitive multiplexed sensing, Anal. Chem. 91 (2019) 8123–8128.
[5] Z. Chen, Proximity recognition and polymerase-powered DNA walker for one step and amplified electrochemical protein analysis, Biosens. Bioelectron. 128 (2019) 104–112.
[6] X. Zhou, W. Zhang, Z. Wang, J. Han, S. Chen, Ultrasensitive aptasensing of insulin based on hollow porous C3N4/S2O8 2/AuPtAg ECL ternary system and DNA walker amplification, Biosens. Bioelectron. 148 (2019) 111795.
[7] Z. Liu, S. Lei, L. Zou, G. Li, L. Xu, B. Ye, Highly ordered 3D electrochemical DNA biosensor based on dual orientation controlled rolling motor and graftable tetrahedron DNA, Biosens. Bioelectron. 147 (2020) 111759.
[8] M. Qing, S. Xie, W. Cai, D. Tang, Y. Tang, J. Zhang, R. Yuan, Click Chemistry

reaction-triggered 3D DNA walking machine for sensitive electrochemical detection of copper ion, Anal. Chem. 90 (2018) 11439–11445.
[9] W. Kun, H. Meng-Qi, Z. Fu-Heng, J. Rong-Huan, Y. Yong-Liang, Autonomous DNA nanomachine based on cascade amplification of strand displacement and DNA walker for detection of multiple DNAs, Biosens. Bioelectron. 105 (2018) 159–165.
[10] D. Li, Y. Xu, L. Fan, B. Shen, W. Chen, Target-driven rolling walker based electrochemical biosensor for ultrasensitive detection of circulating tumor DNA using doxorubicin@tetrahedron-Au tags, Biosens. Bioelectron. 148 (2019) 111826.
[11] Y. Nie, X. Zhang, Q. Zhang, Z. Liang, Q. Ma, X. Su, A novel high efficient electrochemiluminescence sensor based on reductive Cu(I) particles catalyzed Zn-doped MoS2 QDs for HPV 16 DNA determination, Biosens. Bioelectron. 160 (2020) 112217.
[12] L. JiaLi, T. ZhiLing, Z. JiaQi, C. YaQin, Z. Ying, Morphology-Controlled 9,10-diphenylanthracene nanoblocks as electrochemiluminescence emitters for MicroRNA detection with one-step DNA walker amplification, Anal. Chem. 90 (2018) 5298–5305.
[13] R. Zhang, Y. Wang, X. Qu, S. Li, Y. Zhao, S. Liu, J. Huang, Exonuclease III-powered DNA walking machine for label-free and ultrasensitive electrochemical sensing of antibiotic, Sensor. Actuator. B Chem. 297 (2019) 126771.
[14] C. Jung, P.B. Allen, A.D. Ellington, A simple, cleated DNA walker that hangs on to surfaces, ACS Nano 11 (2017) 8047–8054.
[15] Z. Xu, Y. Chang, Y. Chai, H. Wang, R. Yuan, Ultrasensitive electrochemiluminescence biosensor for speedy detection of microRNA based on a DNA rolling machine and target recycling, Anal. Chem. 91 (2019) 4883–4888.
[16] P. Miao, Y. Tang, Gold nanoparticles-based multipedal DNA walker for ratiometric detection of circulating tumor cell, Anal. Chem. 91 (2019) 15187–15192.
[17] K. Mayura, R. Parker, W.O. Berndt, T.D. Phillips, Ochratoxin A-induced teratogenesis in rats: partial protection by phenylalanine, Appl. Environ. Microbiol. 48 (1984) 1186–1188.
[18] Annie Pfohl-Leszkowicz, A. Richard, Ochratoxin A. Manderville, An overview on toxicity and carcinogenicity in animals and humans, Mol. Nutr. Food Res. 51 (2007) 61–99.
[19] Y.-J. Yang, Y. Zhou, Y. Xing, G.-M. Zhang, Y. Zhang, C.-H. Zhang, P. Lei, C. Dong, X. Deng, Y. He, A Label-free aptasensor based on Aptamer/NH2 Janus particles for ultrasensitive electrochemical detection of Ochratoxin A, Talanta 199 (2019) 310–316.
[20] X. Wang, Y. Shan, M. Gong, X. Jin, L. Lv, M. Jiang, J. Xu, A novel electrochemical sensor for ochratoxin A based on the hairpin aptamer and double report DNA via multiple signal amplification strategy, Sensor. Actuator. B Chem. B281 (2019) 595–601.
[21] T.P. Lee, B. Saad, E.P. Ng, B. Salleh, Zeolite Linde Type L as micro-solid phase extraction sorbent for the high performance liquid chromatography determination of ochratoxin A in coffee and cereal, J. Chromatogr., A 1237 (2012) 46–54.
[22] M.A. Andrade, F.M. Lancas, Determination of Ochratoxin A in wine by packed in-tube solid phase microextraction followed by high performance liquid chromatography coupled to tandem mass spectrometry, J. Chromatogr., A 1493 (2017) 41–48.
[23] Y. Zhang, L. Wang, X. Shen, X. Wei, X. Huang, Y. Liu, X. Sun, Z. Wan, Y. Sun, Z. Xu, Broad-specificity immunoassay for simultaneous detection of ochratoxins A, B, and C in millet and maize, J. Agric. Food Chem. 65 (2017) 4830–4838.
[24] X. Jie, L. Wei, L. Rui, Y. Yi, Q. Lin, J. Xu, S. Peng, Z. Qian, Z. Yue, Z. Han, Ultrasensitive low-background multiplex mycotoxin chemiluminescence immunoassay by silica-hydrogel photonic crystal microsphere suspension arrays in cereal samples, Sensor. Actuator. B Chem. b232 (2016) 577–584.
[25] X. Song, Y. Wang, S. Liu, X. Zhang, J. Wang, H. Wang, F. Zhang, J. Yu, J. Huang, A triple amplified electrochemical biosensor for lead ion assay coupling with DNAzyme and catalytic hairpin assembly-induced the formation of 3D DNA-AuNP network, Mikrochim. Acta 186 (2019) 559.
[26] Y.H. Wang, Y.X. Chen, X. Wu, K.J. Huang, Electrochemical biosensor based on Se-doped MWCNTs-graphene and Y-shaped DNA-aided target-triggered amplification strategy, Colloids Surf. B Biointerfaces 172 (2018) 407–413.
[27] Z. Yang, S. Zhang, H. Zhao, H. Niu, Z.-S. Wu, H.-T. Chang, Branched DNA junction-enhanced isothermal circular strand displacement polymerization for intracellular imaging of MicroRNAs, Anal. Chem. 90 (2018) 13891–13899.
[28] Z. Qing, X. He, J. Huang, K. Wang, Z. Zou, T. Qing, Z. Mao, H. Shi, D. He, Target-catalyzed dynamic assembly-based pyrene excimer switching for enzyme-free nucleic acid amplified detection, Anal. Chem. 86 (2014) 4934–4939.
[29] L. Wei, C. Anyi, L. ShengKai, P. KanFu, C. YaQin, Y. Ruo, A novel perylene derivative/luminol nanocomposite as strong electrochemiluminescence emitter for construction of ultrasensitive MicroRNA biosensor, Anal. Chem. 91 (2018) 1516–1523.
[30] C. Hua, M. Peng, Bipedal DNA walker based electrochemical genosensing strategy, Anal. Chem. 91 (2019) 4953–4957.
[31] L. Li, N. ChangChun, L. Tian, W. YaFang, Z. Ying, W. HaiJun, Y. Ruo, L. Pu, Ultrasensitive electrochemiluminescence biosensor for detection of laminin based on DNA dendrimer-carried luminophore and DNA nanomachinemediated target recycling amplification, Biosens. Bioelectron. 101 (2017) 206–212.
[32] G. Liang, X. Liu, G-quadruplex based impedimetric 2-hydroxyfluorene biosensor using hemin as a peroxidase enzyme mimic, Microchimica Acta 182 (2015) 2233–2240.
[33] K. Pei, Y. Xiong, B. Xu, K. Wu, X. Li, H. Jiang, Y. Xiong, Colorimetric ELISA for ochratoxin A detection based on the urease-induced metallization of gold nanoflowers, Sensor. Actuator. B Chem. 262 (2018) 102–109.
[34] L. Yi, X. Huang, X. Chen, W. Zhang, P. Guo, Y. Xiong, Plasmonic ELISA for naked-eye detection of ochratoxin A based on the tyramine-H2O2 amplification system, Sensor. Actuator. B Chem. B259 (2018) 162–169.
[35] S. Wang, Y. Zhang, G. Pang, Y. Zhang, S. Guo, Tuning the aggregation/disaggregation behavior of graphene quantum dots by structure-switching aptamer for high-sensitivity fluorescent ochratoxin A sensor, Anal. Chem. 89 (2016) 1704–1709.
[36] S. Wu, N. Duan, X. Ma, Y. Xia, H. Wang, Z. Wang, Q. Zhang, Multiplexed fluorescence resonance energy transfer aptasensor between upconversion nanoparticles and graphene oxide for the simultaneous determination of mycotoxins, Anal. Chem. 84 (2012) 6263–6270.
[37] S. Peng, L. Wei, L. Yan, D. Zhi, D. Yang, High-throughput low-background GQuadruplex aptamer chemiluminescence assay for ochratoxin A using a single photonic crystal microsphere, Anal. Chem. 89 (2017) 11862–11868.
[38] J. Ni, W. Yang, Q. Wang, F. Luo, L. Guo, B. Qiu, Z. Lin, H. Yang, Homogeneous and label-free electrochemiluminescence aptasensor based on the difference of electrostatic interaction and exonuclease assisted target recycling amplification, Biosens. Bioelectron. 105 (2018) 182–187.
[39] Y. Wang, G. Ning, Y. Wu, S. Wu, B. Zeng, G. Liu, X. He, K. Wang, Facile combination of beta-cyclodextrin host-guest recognition with exonuclease-assistant signal amplification for sensitive electrochemical assay of ochratoxin A, Biosens. Bioelectron. 124–125 (2018) 82–88.
[40] M. Nan, Y. Bi, H. Xue, S. Xue, H. Long, L. Pu, G. Fu, Rapid determination of ochratoxin A in grape and its commodities based on a label-free impedimetric aptasensor constructed by layer-by-layer self-assembly, Toxins 11 (2019) 71.